

# Magnetic Field Tomography with a Directional Analog to the Hanle Effect

Jarom S. Jackson\* and Dallin S. Durfee†

*Department of Physics and Astronomy, Brigham Young University, Provo, Utah 84602*

We discuss an effect analogous to the Hanle effect, but involving the directionality rather than the polarization of scattered light. The effect is important to understand light scattered in the presence of magnetic fields. It can be utilized for field metrology, similar to the traditional Hanle effect, but using a simpler detector, and having immunity to polarization-altering properties of the medium between the probed region and the optical sensor. This method is particularly well suited for characterizing magneto-optical traps, as demonstrated by field tomography of a strontium trap.

In 1924, Wilhelm Hanle presented a theory explaining the depolarization of light scattered by an atomic vapor in a magnetic field. This effect, known as the “Hanle” effect, has been used to determine lifetimes of atomic states [1], to measure or place bounds on magnetic fields [2, 3], and to measure phenomena related to magnetic fields [4, 5]. Other manifestations associated with the Hanle effect have also been utilized, such as a measurement of a “mechanical” Hanle effect [6].

We report on a “directional” Hanle effect—a magnetic field-induced alteration of spatial emission patterns. Understanding this effect is crucial to correctly interpret light scattered in the presence of a magnetic field. Similar to the traditional Hanle effect, it can be used to measure lifetimes and fields without the need of a physical sensor, other than the atoms themselves, in the field region. Applications of the directional Hanle effect are possible in astrophysics, laboratory plasmas, and other disciplines where Hanle effect-related techniques been developed [7–9] or proposed [10–12].

The directional Hanle effect has the added advantage over the classical Hanle effect of requiring no polarizing elements in the detector, and being less susceptible to birefringence and other polarization-altering properties of the medium between the measurement region and the detector. While other fluorescence-based field measurements have been demonstrated [13, 14], this effect is particularly well suited for field characterization in a magneto-optical trap (MOT), as it requires little equipment and setup beyond what is needed to create a MOT, and is most sensitive to fields with strengths typical of those in MOTs. We demonstrate this technique by mapping fields in a strontium MOT.

The traditional Hanle effect can be understood by treating atoms as classical oscillating electric dipoles. Light induces an electric dipole moment along the polarization axis. But in the presence of a magnetic field, the oscillation axis will rotate with time, changing the polarization of the radiated light. In steady state, atoms are spread over a distribution of decay state and rotation angle. If many rotations happen within the decay time, appreciable radiation will come from atoms in all orientations, and the scattered light will be unpolarized.

In addition to depolarization, a magnetic field also

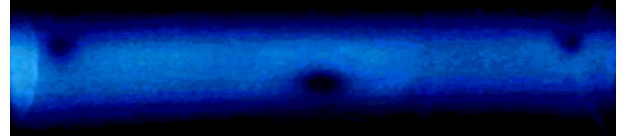


Figure 1. Fluorescence from strontium atoms in an inhomogeneous magnetic field. A thermal strontium vapor was illuminated with a thin sheet of resonant laser light. With the laser polarization set along the line from the atoms to the camera, zero points in the field are clearly visible as dark spots. The width of these dark spots is related to the local field gradients. (color online)

changes the spatial radiation pattern of the scattered light. With no magnetic field, atoms will fluoresce into a sine-squared dipole emission pattern, and no light will be emitted in the direction of the driving light polarization. But if a field is applied, the emission pattern rotates. The amount of light detected by an observer along the polarization axis will depend on how far the dipoles rotate before decaying, which, in turn, depends on the magnetic field strength. An example of this can be seen in Fig. 1, which shows fluorescence from atoms in a region with 3 field zero points[15].

To determine magnetic fields from an image like the one in Fig. 1, we model radiation fields classically, but quantize atomic energy levels. We assume an atom with a  $j = 0$  ground and a  $j = 1$  excited state, as is the case for the  $5s^2\ ^1S_0$  to  $5s5p\ ^1P_1$  resonance transition in strontium. Zeeman shifts split the upper state degeneracy, causing scattered light contributions from the sublevels to change phase with time. This changes the radiation field in time in a way analogous to the field of a classical oscillating dipole with a drifting oscillation axis.

If the atom is excited to a superposition of excited-state magnetic sublevels,  $|\Psi\rangle = a_0|0\rangle + a_-|-1\rangle + a_+|1\rangle$ , the scattered light field is the sum of classical oscillating dipole fields weighted by the amplitude coefficients  $a_0$ ,  $a_-$ , and  $a_+$ . The initial magnitudes of these amplitudes

right after absorbing light are

$$\begin{aligned} |a_0| &= \sqrt{\frac{R_0}{R_t}} \cos \theta_l \quad \text{and} \\ |a_{\pm}| &= \sqrt{\frac{R_{\pm}}{2R_t}} \sin \theta_l, \end{aligned} \quad (1)$$

where  $\theta_l$  is the angle between the laser polarization and the  $z$  axis, and the parameter

$$R_{0,\pm} = \frac{I_L}{I_s} \left( \frac{\Gamma/2}{1 + I_L/I_s + 4\delta_{0,\pm}^2/\Gamma^2} \right), \quad (2)$$

is an off-resonance transition rate, which depends on the transition linewidth  $\Gamma$  and the detuning  $\delta_{0,\pm}$  (a sum of the laser offset from the zero-field resonance, Zeeman shifts, and Doppler shifts).  $I_L$  is the intensity of the driving light,  $I_s$  is the saturation intensity of the transition, and

$$R_t = \cos^2 \theta_l R_0 + \frac{1}{2} \sin^2 \theta_l (R_+ + R_-). \quad (3)$$

The far-field radiation field  $\mathbf{E}(\mathbf{r})$  at a displacement  $\mathbf{r}$  from a classical dipole oscillating at an angular frequency  $\omega$  and decaying according to a linewidth  $\Gamma$  is given by

$$\mathbf{E}(\mathbf{r}) = \frac{\omega^2}{4\pi\epsilon_0 c^2 r} (\hat{\mathbf{r}} \times \mathbf{d}) \times \hat{\mathbf{r}} e^{-\Gamma t_r/2} e^{-i\omega t_r}. \quad (4)$$

Here  $c$  is the speed of light,  $\epsilon_0$  is the permittivity of free space, and  $t_r = t - r/c$  is the retarded time. The vector  $\mathbf{d}$  takes one of the values

$$\begin{aligned} \mathbf{d}_0 &= d_0 \hat{\mathbf{z}} & (m=0) \\ \mathbf{d}_{\pm} &= \frac{1}{\sqrt{2}} d_0 (\hat{\mathbf{x}} \pm i\hat{\mathbf{y}}) & (m=\pm 1) \end{aligned} \quad (5)$$

to describe a dipole oscillating with an amplitude  $d_0$  along the  $z$  axis (analogous to an atom radiating from the  $m=0$  sublevel), or a dipole of magnitude  $d_0/\sqrt{2}$  rotating around the  $z$  axis (analogous to an atom radiating from the  $m=1$  or  $m=-1$  sublevel). The parameter  $d_0$  can be related to the matrix element for the transition [15]. We assume all upper state sublevels decay with the same linewidth.

Zeeman shifts are typically minute compared to the atomic resonance frequency, so they will be neglected in the field amplitudes. But Zeeman shifts in the complex exponential factor in Eq. 4 cause the relative phases of the field contributions to change in time, changing the radiation pattern, and generating the directional Hanle effect. We will use the Zeeman shifted frequencies  $\omega_0$  and  $\omega_{\pm} = \omega_0 \pm \Delta\omega$ . Here  $\Delta\omega = \mu_B g B/\hbar$ , where  $\mu_B$  is the Bohr magneton,  $B$  is the local field magnitude, and  $g$  is the Landé g-factor ( $g=1$  for the  $5s5p \ ^1P_1$  state in strontium).

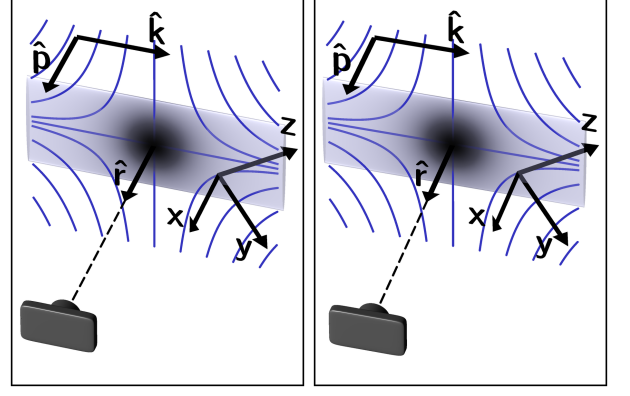


Figure 2. Illustration of the coordinate system (3D stereoscopic pair for cross-eyed viewing). The sheet of laser light is depicted by a rectangle. The camera is shown in the lower left-hand corner. The dark area in the center depicts the low field region from which little light scatters in the  $\hat{\mathbf{p}}$  direction. The curved paths represent magnetic field lines. The field direction defines the local  $z$  axis, and  $x$  is defined to be in the  $\hat{\mathbf{p}} = \hat{\mathbf{r}}$  direction, which is orthogonal to the laser propagation direction  $\hat{\mathbf{k}}$ . (color online)

The total scattered field for a single atom is, then

$$\begin{aligned} \mathbf{E}_{\text{atom}}(\mathbf{r}) &= E_r e^{-\Gamma t_r/2} \left[ a_0 (\hat{\mathbf{r}} \times \hat{\mathbf{z}}) \times \hat{\mathbf{r}} e^{-i\omega_0 t_r} \right. \\ &\quad + a_+ \left( \hat{\mathbf{r}} \times \frac{1}{\sqrt{2}} (\hat{\mathbf{x}} + i\hat{\mathbf{y}}) \right) \times \hat{\mathbf{r}} e^{-i\omega_+ t_r} \\ &\quad \left. + a_- \left( \hat{\mathbf{r}} \times \frac{1}{\sqrt{2}} (\hat{\mathbf{x}} - i\hat{\mathbf{y}}) \right) \times \hat{\mathbf{r}} e^{-i\omega_- t_r} \right], \end{aligned} \quad (6)$$

where  $E_r = \omega_0^2 d_0 / 4\pi\epsilon_0 c^2 r$ .

In principle, the field radiated by an ensemble of atoms can be found by integrating the single atom intensity,  $I_{\text{atom}} = \frac{1}{2} c \epsilon_0 |\mathbf{E}_{\text{atom}}|^2$ , over the distribution of Doppler-dependent transition rates and the retarded time (excited atoms are in different stages of decay). Analytical calculations can become prohibitively complex at this point, so we will proceed with a limited case involving certain assumptions. Later we present results of a more complete numerical model.

First, we assume the atoms are driven by a thin sheet of laser light, polarized in a direction  $\hat{\mathbf{p}}$  which is normal to the sheet, and that within the light sheet the local magnetic field direction,  $\hat{\mathbf{z}}$ , lies within the plane of the sheet. This will be the case near the field zero in the center of a spherical quadrupole field if the light sheet passes through the zero. With these assumptions,  $\theta_l = \pi/2$  radians. We also assume the direction from the atoms to the detector,  $\hat{\mathbf{r}}$ , is parallel to  $\hat{\mathbf{p}}$ . This is the direction in which the effect is most pronounced. We define this to be the  $x$  direction, as shown in Fig. 2.

Our final assumption is that  $R_0 = R_+ = R_-$ , and that these rates are the same for every atom in the ensemble. This assumption is not generally accurate. In the case

of broadband or strongly saturating driving light, it is approximately true. Even when it is not a good approximation, it allows us to find a simple analytical expression to aid intuition. Furthermore, we show later that including the full rate expressions makes only a small difference in our experiment.

With these assumptions, the amplitude coefficients become  $a_0 = 0$  and  $a_{\pm} = 1/\sqrt{2}$ , and Eq. 6 can be simplified to

$$\mathbf{E}_{\text{atom}}(\mathbf{r}) = E_r \sin(\Delta\omega t_r) e^{-\Gamma t_r/2} e^{-i\omega_0 t_r} \hat{\mathbf{y}}. \quad (7)$$

The intensity radiated on the polarization axis by a single atom is

$$I_{\text{atom}} = I_r \sin^2(\Delta\omega t_r) e^{-\Gamma t_r}, \quad (8)$$

where  $I_r = c\epsilon_0 E_r^2/2$ .

To get an ensemble averaged intensity, we integrate this over  $t_r$  from 0 to  $\infty$ . The result is an inverted Lorentzian curve,

$$\langle I_{\text{ensemble}} \rangle = I_H \left[ 1 - \frac{1}{1 + \frac{4\mu_B^2 g^2}{\hbar^2 \Gamma^2} B^2} \right], \quad (9)$$

where  $I_H$  is a constant which depends on the driving light intensity and the number of atoms being driven.

From this equation we see that in the limit of zero magnetic field, no light is emitted in this direction. As the field increases, the intensity grows, approaching an asymptotic limit of  $I_H$ . The full-width, half-maximum width of this curve is

$$B_{\text{FWHM}} = \hbar\Gamma/\mu_B g. \quad (10)$$

Because of the shallow slope of the curve near zero field and the asymptotic saturation at high fields, field measurements using the directional Hanle effect are most precise for field magnitudes on the order of  $B_{\text{FWHM}}$ . This is, fortunately, the scale of the fields present in a typical MOT's trapping region.

The expression in Eq. 9 is graphed in Fig. 3, along with numerically calculated curves that don't assume equal transition rates. In the analytical model, laser intensity, detuning, and Doppler shifts only impact  $I_H$ . When rate effects are accounted for, these factors are more important. In the rate-dependent model we assumed a thermal strontium beam from an oven with a temperature of 500° C, and assumed the laser was tuned to cancel the Doppler shift at the peak of the velocity distribution.

Fig. 3 shows that the analytical solution is a good qualitative representation of the effect, deviating from the full model by only a few percent. Discrepancies are smaller with higher driving light intensity. Doppler shifts in the rate-dependent model cause scattered intensity to increase somewhat faster with field strength than in the Lorentzian model; unequal rates to the Zeeman-shifted

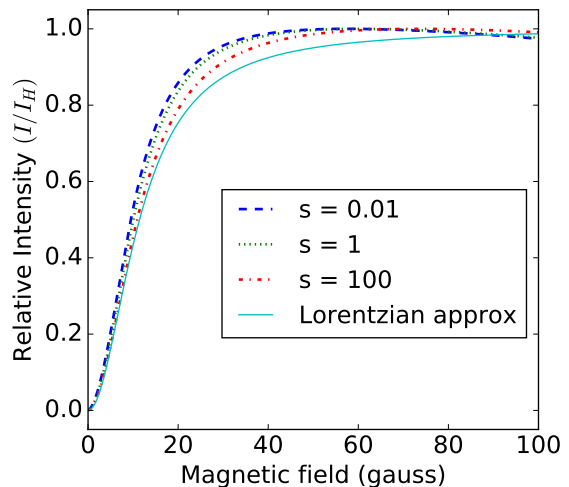


Figure 3. Four curves comparing models of the light emitted along the polarization axis. The first three are numerical calculations, representing results at various light intensities ( $s$  is the assumed saturation parameter). The fourth is the Lorentzian solution (Eq. 9) which assumes equal excitation rates for the magnetic sublevels. (color online)

sublevels cause one of the states to scatter more than the other, making complete cancellation of the emissions impossible.

If the laser intensity distribution, the atomic density, and the velocity distribution are not well known, one only needs to detect scattering from a large field region to determine  $I_H$  in the Lorentzian model. In the numerical model, the curves reach a maximum and then drop off as Zeeman shifts push atoms out of resonance. Calibration can be done with measurements over a range of fields that pass through the scattering maximum. In practice, if Doppler broadening is large compared to the transition linewidth, the maximum intensities in the models are nearly identical.

We used the directional Hanle effect to characterize the field in a strontium MOT [16]. We blocked all but one laser beam, and inserted a polarizer and a narrow slit into the remaining beam. The light was aligned to pass through the field zero in the center of the chamber by adjusting its position to make the dark spot in the image as large and dark as possible. The camera, a webcam [17] with internal processing disabled [18, 19], was placed outside the vacuum chamber about 10 cm from the trap, in a direction perpendicular to the light sheet and parallel to the polarization direction, as shown in Fig. 2

The magnetic fields in our MOT are generated by a pair of opposing permanent ring magnets which produce a field zero midway between them as well as a second, ring shaped zero crossing. The central zero point, as well as two points where the image plane intersects the zero-field ring, are clearly visible as dark spots in the fluorescence

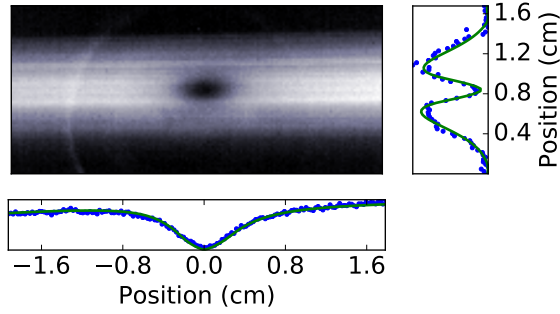


Figure 4. Image of the dark spot corresponding to the zero point in our trapping potential, along with profile plots of the image (blue dots) and the model fit (green curves). (color online)

shown in Fig. 1. The fact that the spots were not in a line revealed a previously unknown asymmetry in the trap (probably due to a magnet that had been weakened when accidentally heated).

The field near the center of our MOT should approximate a spherical quadrupole field, having the form  $\mathbf{B} = B'(x\hat{\mathbf{x}} + y\hat{\mathbf{y}} - 2z\hat{\mathbf{z}})$ . Here we have abandoned the coordinate system used to derive Eq. 9 and used a system in which  $z$  is the symmetry axis of our magnets (the vertical direction in Figs. 1 and 4), and the  $x$  direction is the direction of the light sheet propagation (the horizontal direction in the figures). The parameter  $B'$  is a constant, representing the field gradient in the  $x$  or  $y$  direction.

We fit images, such as the one in Fig. 4, to three different models of light scattering. Our simplest data analysis assumed the Lorentzian model in Eq. 9. A more complicated analytical model included effects due to the small deviations of the  $\hat{\mathbf{r}}$  direction over the image. For both of these fits we assumed a Gaussian laser profile in the  $z$  direction. The Gaussian width and the  $z$  offset of the beam were free fit parameters, as was the largest signal we would detect at the peak of the Gaussian in the limit of high magnetic field.

For the two analytical models, we assumed the field magnitude in the region had the form  $|B| = [B'_x(x - x_0)^2 + B'_z(z - z_0)^2]^{0.5}$ , where  $B'_x$  and  $B'_z$  are the magnitudes of the field gradients in the  $x$  and  $z$  directions, and  $x_0$  and  $z_0$  are the location of the field zero. Because all the data points are in the  $y = 0$  plane, there was no  $y$  gradient term. Using independent fit parameters for the two gradients allowed us to gain additional insight into the accuracy of the method by comparing the ratio  $B'_z/B'_x$  to the expected ratio of 2 for a spherical quadrupole field.

The third model was a numerical model that kept the assumption that  $\hat{\mathbf{r}} = \hat{\mathbf{p}}$ , but did not make the equal rate approximation (Eq. 7). This model is affected by Doppler

Model	$ B'_x $ (G/cm)	$ B'_z $ (G/cm)
Simple Lorentzian model	$35.92 \pm 0.26$	$70.29 \pm 0.53$
Analytic, no $\hat{\mathbf{r}} = \hat{\mathbf{p}}$ assumption	$36.74 \pm 0.28$	$70.23 \pm 0.55$
Numerical, $s_0 = 1.4$	$30.31 \pm 0.17$	$67.44 \pm 0.49^*$
Numerical, $s_0 = 0.1$	$28.74 \pm 0.17$	$64.03 \pm 0.46$
Hall probe measurement		$67.3^*$
Permanent magnet calculation		69.0

Table I. Tabulated results for the magnetic field gradients in  $x$  and  $z$  directions, as well as the least square fitting errors, calculated from the data in Fig. 4. \*The most accurate result should be from the numerical model (which uses the most complete theory), and the more accurate of the predicted values should be the Hall probe measurement.

shifts, so the ensemble integral becomes a double integral over time and velocity distribution. As with the numerical curves in Fig. 3, we assumed a thermal beam from a 500° C oven. We adjusted the laser frequency to maximize the visual fluorescence, and assumed the laser detuning exactly canceled the Doppler shift at the peak of the thermal distribution.

In the numerical model we fit the field to third-order polynomials in  $x$  and  $z$  to better approximate the field at larger distances from the field zero. We also included fit parameters to account for slight misalignment of the image  $z$  direction from the field symmetry axis, and to linearly model a small drop in laser intensity across the atoms. We manually set a peak saturation parameter  $s_0$ . Measurements of the laser beam suggested a saturation parameter near unity at the peak of the Gaussian intensity distribution. The best fit occurred with  $s_0 = 1.4$ . Comparing to a fit assuming  $s_0 = 0.1$  shows that the method is fairly insensitive to assumed light intensity.

Results are tabulated in Table I. The table also includes two independent estimates of the  $z$  gradient. The first was calculated using the theoretical surface current for the type of permanent magnets in our setup. The second is a Hall probe measurement made on each magnet outside of the setup. Even the simple model compares well with the expected gradients. Figure 4 shows an image along with profile plots of both the data and the model.

In conclusion, we discussed a magnetic-field induced change in scattered light directionality, related to the Hanle effect. Using this phenomenon we can measure fields without any polarization measurements. The method is most sensitive to fields of the size typically found in MOTs, requires little additional equipment or setup, and does not require a physical probe in the vacuum (other than the atoms themselves), making it useful for MOT characterization. We used this technique to locate the zero-field points and measure field gradients in a strontium MOT. This work was supported by NSF grant No. PHY1205736.

---

\* jaromsj@physics.byu.edu

† dallin\_durfee@byu.edu

- [1] Giovanni Moruzzi and Franco Strumia. *The Hanle effect and level-crossing spectroscopy*. Springer Science & Business Media, 2013.
- [2] Alfred Kastler. The Hanle effect and its use for the measurements of very small magnetic fields. *Nuclear Instruments and Methods*, 110:259–265, 1973.
- [3] Cédric Roux, Andreas Emmert, Adrian Lupascu, Thomas Nirrengarten, Gilles Nogues, Michel Brune, J-M Raimond, and Serge Haroche. Bose-Einstein condensation on a superconducting atom chip. *Europhysics Letters*, 81(5):56004, 2008.
- [4] Mark Johnson and R. H. Silsbee. Interfacial charge-spin coupling: Injection and detection of spin magnetization in metals. *Physical Review Letters*, 55:1790–1793, 1985.
- [5] L. O’Brien, D. Spivak, N. Krueger, T. A. Peterson, M. J. Erickson, B. Bolon, C. C. Geppert, C. Leighton, and P. A. Crowell. Observation and modeling of ferromagnetic contact-induced spin relaxation in Hanle spin precession measurements. *Phys. Rev. B*, 94:094431, 2016.
- [6] R. Kaiser, N. Vansteenkiste, A. Aspect, E. Arimondo, and C. Cohen-Tannoudji. Mechanical Hanle effect. *Zeitschrift für Physik D Atoms, Molecules and Clusters*, 18(1):17–24, 1991.
- [7] J. O. Stenflo. The Hanle effect and the diagnostics of turbulent magnetic fields in the solar atmosphere. *Solar Physics*, 80(2):209–226, 1982.
- [8] J. O. Stenflo, C. U. Keller, and A. Gandorfer. Differential Hanle effect and the spatial variation of turbulent magnetic fields on the Sun. *Astronomy and Astrophysics*, 329:319–328, 1998.
- [9] V. Bommier. Quantum theory of the Hanle effect. II-effect-effect of level-crossings and anti-level-crossings on the polarization of the D3 helium line of solar prominences. *Astronomy and Astrophysics*, 87:109–120, 1980.
- [10] R. Presura. Hanle effect as candidate for measuring magnetic fields in laboratory plasmas. *Review of Scientific Instruments*, 83(10):10D528, 2012.
- [11] R. Ignace, K. H. Nordsieck, and J. P. Cassinelli. The Hanle effect as a diagnostic of magnetic fields in stellar envelopes. I. theoretical results for integrated line profiles. *The Astrophysical Journal*, 486:550–570, 1997.
- [12] R. Ignace. The Hanle effect as a diagnostic of magnetic fields in stellar envelopes. V. thin lines from Keplerian disks. *The Astro*, 725:1040–1052, 2010.
- [13] Ph.W. Courteille, S.R. Muniz, K. Magalhães, R. Kaiser, L.G. Marcassa, and V.S. Bagnato. Magnetic field tomography. *The European Physical Journal D - Atomic, Molecular, Optical and Plasma Physics*, 15(2):173–180, 2001.
- [14] C. V. Nielsen, J. K. Lyngsø, A. Thorseth, M. Galouzis, K. T. Therkildsen, E. D. van Ooijen, and J. W. Thomsen. Characterization of a magnetic trap by polarization dependent Zeeman spectroscopy. *The European Physical Journal D*, 48(1):111–119, 2008.
- [15] Jarom Silver Jackson. In situ magnetic field characterization with the directional Hanle effect. Master’s thesis, Brigham Young University, 2016.
- [16] Christopher Joseph Erickson. *Development of a Strontium-87 Ion Interferometer*. PhD thesis, Brigham Young University, 2011.
- [17] A Logitech QuickCam Pro 9000.
- [18] Lisa M. Richards, S. M. Shams Kazmi, Janel L. Davis, Katherine E. Olin, and Andrew K. Dunn. Low-cost laser speckle contrast imaging of blood flow using a webcam. *Biomed. Opt. Express*, 4(10):2269–2283, Oct 2013.
- [19] Gregor Langer, Armin Hochreiner, Peter Burgholzer, and Thomas Berer. A webcam in Bayer-mode as a light beam profiler for the near infra-red. *Optics and Lasers in Engineering*, 51(5):571 – 575, 2013.